analytical chemistry

Article

pubs.acs.org/ac

Probing Biomolecular Interactions with Dual Polarization Interferometry: Real-Time and Label-Free Coralyne Detection by Use of Homoadenine DNA Oligonucleotide

Yong Wang,[†,‡] Juan Wang,[†,‡] Fan Yang,[†] and Xiurong Yang*[,†]

[†]State Key Laboratory of Electroanalytical Chemistry, Changchun Institute of Applied Chemistry, Chinese Academy of Sciences, Changchun, Jilin 130022, China

[‡]Graduate School of the Chinese Academy of Sciences, Beijing 100039, China

Supporting Information

ABSTRACT: We incorporated the specific recognition of adenine-rich singled-stranded DNA (ssDNA) into dual polarization interferometry (DPI) measurements for direct, selective, and sensitive detection of the small molecule coralyne, and we simultaneously employed the real-time and label-free technique for detailed investigation of the interaction between coralyne and adenine-rich ssDNA. Data from UV−visible spectroscopy, circular dichroism (CD) spectroscopy, and DNA melting firmly confirmed that 48-mer homoadenine ssDNA oligonucleotide (A_{48}) had highly specific recognition for coralyne, whereas 48-mer homothymine ssDNA oligonucleotide (T_{48}) as the control had no such recognition. The immobilization of ssDNA (A_{48} or T_{48}) on a silicon oxynitride chip could be achieved through a preadsorbed poly(ethylenimine) (PEI) layer. Mass, thickness, and refractive index (RI) changes resolved by DPI during the whole process of ssDNA immobilization suggested that most ssDNA molecules were likely to lie on the PEI surface mainly in the form of a flat monolayer and insert themselves partly into the PEI layer. Qualitative and quantitative analysis of mass, thickness, and RI changes in A_{48}/PEI layer upon addition of different concentrations of coralyne revealed that A_{48} most likely underwent a conformational change from single-stranded to double-stranded structure. By evaluation of the binding curves from changes in mass, the association rate constant (k_a), dissociation rate constant (k_d), and association constant (K_A) between coralyne and A_{48} were determined to be 4.95×10^3 M^{-1} s^{-1}, 0.031 s^{-1}, and 1.6×10^5 M^{-1}, respectively. Good linear correlations between coralyne concentrations ranging from 0.5 to 12 μM and three parameters (mass, thickness, and RI) resolved by the response to coralyne binding were obtained. The detection limits were 0.22 μM for mass calibration, 0.14 μM for thickness calibration, and 0.32 μM for RI calibration. The high selectivity of the biosensor to coralyne at the A_{48}/PEI interface was successfully confirmed by using the other two interfaces (T_{48}/PEI and PEI) and three typical intercalators (ethidium bromide, daunomycin, and methylene blue). It is expected that the biosensing platform may be extended to simultaneously detect and characterize the interactions of a variety of target molecules with functional DNA molecules with high sensitivity.

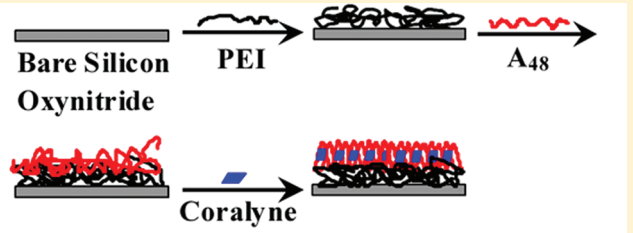

Over the past decades, biosensors have emerged as an increasingly pivotal technology for detection and analysis of the interactions of many biological system from proteins, DNA, oligosaccharides, and lipids to small molecules, phage, viral particles, and cells.[1−4] In general, based on the readout type of transducers, biosensors can be separated into two broad categories involving label-based and label-free detection.[5−8] A large number of applications of biomolecular interactions have employed some type of label-based strategy.[9−13] These methods that involve labeling can achieve high detection sensitivity, but they have several problems and drawbacks. On the one hand, labeling introduces chemical modification and requires additional incubation and washing steps. These steps are not only time-consuming, expensive, and labor-intensive but they also reduce quantitative accuracy. On the other hand, direct attachment of a tag (reporter molecule) to the target molecule or the receptor can alter their structure and possibly perturb the specific binding between the target molecule and the receptor, resulting in reduced sensitivity or selectivity.

All these limitations have driven the development of label-free biosensors for investigating various biomolecular interactions. Very recently, a variety of label-free detection techniques have emerged, including optical,[14−16] electrical,[17−19] and acoustic.[20,21] However, most of these techniques cannot simultaneously provide kinetic, thermodynamic, and structural information on biomolecular interactions. Therefore, the development of a universal means for real-time, label-free biosensing remains a compelling goal.

An evanescent optical biosensing platform based on dual polarization interferometry (DPI) technique has previously

Received: July 29, 2011
Accepted: December 8, 2011
Published: December 8, 2011

   dx.doi.org/10.1021/ac2019443 | *Anal. Chem.* 2012, 84, 924−930

been reported to be a good choice to fulfill the requirements.[22] The technique was developed and commercialized in 2000 by Farfield Group, Ltd..[23] It employs a multiple-layer optical waveguide structure consisting of reference and sensing layers separated by a layer of cladding that mimics the well-known Young's double-slit interference experiment in optics. The technique based on optical interferometry is inherently more sensitive than that based on surface plasmon resonance (SPR)[24−26] and is reported to credibly detect molecules below 50 Da.[27] Moreover, DPI technique utilizes both transverse magnetic (TM) and transverse electric (TE) polarizations and allows the unambiguous determination of change in mass, thickness, and refractive index (RI) in surface layers.[26,28,29] Hence, DPI embodies a truly quantitative analytical technique rather than a simple "mass sensor" response function and can be applied to reveal structural information about the biomolecular interactions taking place as the packing (from RI) and molecule dimension (from layer thickness) change. Also, DPI can typically give a link between a molecule's structure and its function.[26,28] In the past, the technique has been applied for monitoring of protein adsorption,[30] polyelelectrolyte assembly,[31] vesicle deformation,[32] lipid membrane formation,[33] etc. Among them, the studies of DNA molecules have attracted a lot of attention. Lu and co-workers[34] investigated the cationic polymer-mediated DNA immobilization using DPI. Berney and Oliver[35] and Sheehan and co-workers[36] used DPI to characterize surface immobilization and hybridization of DNA oligonucleotides. Caruso and co-workers[37,38] applied DPI to study the assembly process of DNA oligonucleotide multilayer films. Our group probed the interaction of genomic DNA with small molecules using DPI.[39,40] However, there is little research on the interaction of DNA oligonucleotides with small molecules by DPI.

In this work, we utilized the real-time and label-free DPI technique to probe the interaction between the small molecule coralyne and adenine-rich ssDNA. Coralyne (13-methyl [1,3]benzodioxolo[5,6-*c*]-1,3-dioxolo[4,5-*i*]phenanthridium) (MW = 418, Scheme 1), a kind of planar alkaloid, was reported

Scheme 1. Fabrication Process of Biosensing Interface and Detection of Coralyne by the DPI Technique

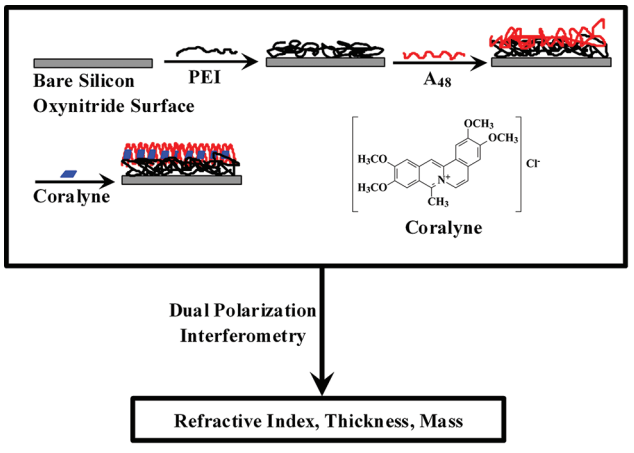

to exhibit antileukemic activity against leukemia L-1210 and P-388, which might be due to the intercalation of coralyne into DNA.[41] In addition, it was also found to function as a kind of topoisomerase inhibitor by stabilizing the complex formed between the enzyme and DNA.[42] Adenine-rich single-stranded DNA (ssDNA) tracts, which exist in most eukaryotes, are nuclease-sensitive regions and are likely to affect chromatin structure by excluding nucleosomes and assisting the entry of transcribing proteins.[43,44] Most recently, coralyne has been reported to bind strongly and specifically to adenine-rich ssDNA and promote its structural transition from single-stranded to double-stranded conformation.[45−48] Thus, investigation of the interaction of coralyne with adenine-rich ssDNA is the fundamental aspect in any attempt to gain a deeper insight into the chemical nature for the interference mechanism of the drug with replication and gene expression in vivo, and furthermore to design and develop other new drug candidates that utilize adenine-rich ssDNA as a target.[49,50] In parallel, we exploited the specific recognition ability of adenine-rich ssDNA by coralyne to fabricate a DPI-based biosensor for direct, selective, and sensitive detection of coralyne based on mass, thickness, and RI changes in the surface layer.

EXPERIMENTAL SECTION

Reagents and Chemicals. Poly(ethylenimine) (PEI, MW = 750 000), 50% (w/v) aqueous solution, and daunomycin hydrochloride (DM) were obtained from Sigma−Aldrich (St Louis, MO). Coralyne chloride hydrate (coralyne) was purchased from Sigma−Aldrich (Milwaukee, WI). Methylene blue (MB) was purchased from Acros Organics. Ethidium bromide was obtained from Continental Laboratory Products Inc. (San Diego, CA). Disodium hydrogen phosphate dodecahydrate (Na_2HPO_4), sodium dihydrogen phosphate dihydrate (NaH_2PO_4), and sodium chloride (NaCl) were purchased from Beijing Chemical Reagent Co. (Beijing, China). The 48-mer homoadenine ssDNA oligonucleotide (A_{48}) and the 48-mer homothymine ssDNA oligonucleotide (T_{48}) were obtained from Sangon Biotechnology Co. Ltd. (Shanghai, China). Unless specified, all other chemicals were of analytical reagent grade and were used without further treatment. Ultrapure water (Milli-Q plus, Millipore Inc., Bedford, MA) was used throughout. Phosphate-buffered saline (PBS, pH 7.4) solutions were prepared with 10 mM NaH_2PO_4−Na_2HPO_4 and 150 mM NaCl. The buffer solution was filtered and degassed before use. Prior to use, ssDNA solutions were prepared by dissolving ssDNA in 10 mM PBS buffer (pH 7.4, with 150 mM NaCl). The concentrations of ssDNA solutions were determined by measuring the 260 nm UV absorbance.

Dual Polarization Interferometry Experiments. The DPI measurements were carried out in real time by use of an AnalLight Bio200 dual polarization interferometer (Farfield Sensors Ltd., Manchester, U.K.). An explanation of the instrument and technique is given in Supporting Information.

Prior to the DPI experiments, the unmodified silicon oxynitride AnalChip was first cleaned with oxidizing piranha solution, a 7:3 mixture of concentrated sulfuric acid and 30% hydrogen peroxide for 15 min. (Caution: Piranha solution is highly corrosive, reactive, and potentially explosive. The solution should be handled using suitable personal protective equipment and proper safety procedures.) After that, the chip was rinsed sequentially by sonication in ultrapure water and ethanol for 10 min. This process was repeated three times. Finally, the chip was dried under a stream of nitrogen gas to remove the water from the surface before it was loaded into the DPI instrument.

In this work, all the DPI experiments were performed at 20 °C in 10 mM PBS running buffer solution (pH 7.4, with 150

dx.doi.org/10.1021/ac2019443 | *Anal. Chem.* 2012, 84, 924−930

mM NaCl). An unmodified silicon oxynitride AnalChip was mounted in the chip carrier and inserted into the DPI instrument, and the PBS running buffer solution was passed through the surface of the chip at a flow rate of 50 μL/min. Once a stable baseline was reached, an 80% (v/v) ethanol/water solution was made to flow over the sensor chip for 4 min, followed by a return to the running buffer solution, allowing the baseline to stabilize once again. After that, an addition of water was conducted in a similar manner. This could be used to calibrate the sensing waveguide thickness and refractive index and the running buffer refractive index. After the calibration procedures, the flow rate was increased to 100 μL/min. A PEI solution (1 mg/mL) was injected for 2 min and incubated for 5 min before returning to the running buffer. Once a stable baseline was attained, a solution of A_{48} (8 μM) or T_{48} (8 μM) was injected for 2 min and incubated for 5 min. The flow was then returned to the running buffer until the DNA/PEI layer had stabilized. After that, coralyne solutions over the concentration range from 0.5 to 20 μM were injected for 2 min. A linearization procedure was performed at the end of the experiment. The linearization was a method for the advanced calibration of the phase response from TM and TE polarizations in order to improve the reliability and consistency of resolved refractive index and thickness. The running buffer was kept at a flow rate of 100 μL/min, and an 80% (v/v) ethanol/water solution was injected to flow over chip surface for 1.5 min. The flow rate of the running buffer was reduced to 15 μL/min after the stable baseline of the 80% (v/v) ethanol/water solution was obtained, to dilute the ethanol/water solution as it flowed over the chip surface.

Determination of refractive index, thickness, and mass per unit area on the biosensor chip surface could be achieved by use of the AnaLight Bio200 analysis software (Farfield Sensors Ltd., Manchester, U.K.).

RESULTS AND DISCUSSION

UV−Visible and Circular Dichroism Spectroscopy Study of Coralyne−ssDNA Binding Principle. Earlier studies demonstrated that adenine-rich ssDNA could recognize coralyne specifically,[45−48] and thymine-rich ssDNA did not possess such specific recognition ability for coralyne.[47,48] Herein, we selected 48-mer homoadenine ssDNA (A_{48}) and 48-mer homothymine ssDNA (T_{48}) as the specific recognition element and the control element for coralyne, respectively, and used UV−visible and circular dichroism (CD) spectroscopy to investigate the binding behaviors of coralyne to the two ssDNA.

Figure S1 (Supporting Information) shows UV−visible absorption spectra of coralyne in the absence and presence of A_{48} or T_{48}. It is clearly noticeable from Figure S1, curve a (Supporting Information), that the spectrum of free coralyne has a peak at 420 nm over the wavelength range 350−500 nm. Upon the addition of T_{48}, the shape and peak location of the coralyne absorption band remained unchanged (Figure S1, curve b, Supporting Information), indicating almost no tight association of coralyne to T_{48}.[46] Different from T_{48}, the addition of A_{48} caused the spectrum of coralyne to undergo dramatic changes, exhibiting three local absorbance maxima at 369, 412, and 435 nm (Figure S1, curve c, Supporting Information). The shift in the wavelength maximum agreed well with the results reported previously,[47] revealing that coralyne induced self-structure involving adenine−adenine base pairing in A_{48} with an intercalative binding geometry.[47]

CD spectra of A_{48} or T_{48} with and without coralyne are presented in Figure S2 (Supporting Information). As can be seen in Figure S2A, A_{48} shows a CD spectrum with a small positive band around 275 nm and an adjacent small negative band around 248 nm, followed by a large positive band at 217 nm, which was highly consistent with that reported in the literature.[46,51] Increasing concentrations of coralyne give rise to pronounced changes in the positive and negative CD bands of A_{48}, resulting in an increase in ellipticity of the negative band around 248 nm, a decrease in ellipticity of the positive band around 217 nm, and an increase in ellipticity of the positive band around 275 nm. These marked changes imply structural alteration of A_{48} upon the binding to coralyne. Concomitant with the band changes in the 210−300 nm region, a very prominent extrinsic CD band appears in the 300−400 nm range with a positive peak around 340 nm and a negative peak around 300 nm (Figure S2A,B, Supporting Information). With the increase of coralyne concentration, the ellipticity of the positive induced band around 340 nm and the negative induced band around 300 nm increases (Figure S2A,B, Supporting Information). Because coralyne lacks any chiral center in its structure and hence has no CD activity, the strong induced CD band in the presence of coralyne confirms the strong chiral environment of intercalated coralyne in the stranded organization of A_{48}.[48] It is worth noting that reduction of the long-wavelength band intensity might be related to the function of both helix winding angle and base pair twist.[43] T_{48} is characterized by a positive band around 280 nm and a negative band around 250 nm (Figure S2C, Supporting Information).[46,51] With increasing concentrations of coralyne, the negative band around 250 nm remains almost unchanged, and the positive band around 280 nm gradually decreases in ellipticity, along with the development of a new band in the 290−360 nm region (Figure S2C,D, Supporting Information). Figure S2C also shows clearly that, in comparison with A_{48}, T_{48} has no induced CD positive band around 340 nm, suggesting no intercalation of coralyne into T_{48}. All these changes are likely to be due to helix winding angle, base pair twist, electrostatic binding of the charged coralyne to the negatively charged phosphates, or changes that occur in the sugar−phosphate backbone.[52]

To further determine the binding ability of A_{48} or T_{48} to coralyne, we employed temperature-dependent CD spectropolarimetry at 340 nm to investigate the melting of A_{48} or T_{48} with and without coralyne (Figure S3, Supporting Information). As can be noted in Figure S3A, there is a sigmoid-shaped cooperative CD melting transition for A_{48}−coralyne with a melting temperature of about 51 °C, which is similar to that of earlier work.[47,48] Notably, no such cooperative CD melting curves are observed for A_{48}, T_{48}, and coralyne−T_{48} (Figure S3B−D, Supporting Information). These results indicate that complexation with coralyne only results in self-structure induction of A_{48}.

Immobilization of ssDNA Monitored by DPI. To successfully probe the interaction of coralyne with ssDNA and further develop the coralyne biosensor, the immobilization of ssDNA on a silicon oxynitride support should be taken into account. To create the surface of ssDNA, we herein followed the electrostatic immobilization approach our group previously described.[39] As displayed in Scheme 1, because the surface of the unmodified silicon oxynitride chip was negatively charged at neural pH (silicon oxynitride has an isoelectric point at pH 3),[53] the unmodified chip was first exposed to PEI (a highly

dx.doi.org/10.1021/ac2019443 | Anal. Chem. 2012, 84, 924−930

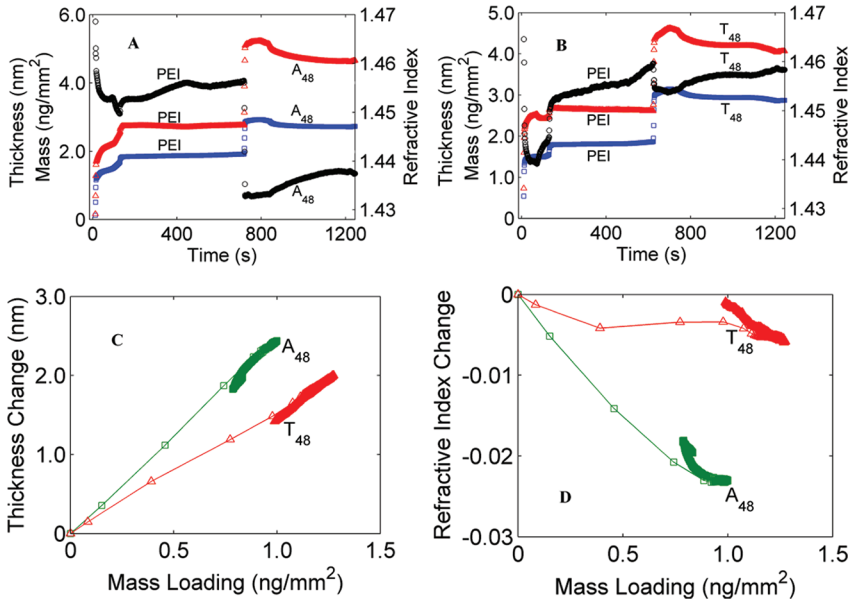

Figure 1. (A) DPI-based temporal evolutions of mass (blue squares), thickness (red triangles), and RI (black circles) during the immobilization of PEI and A_{48} on a bare silicon oxynitride surface. (B) Real-time DPI measurements of mass (blue squares), thickness (red triangles), and RI (black circles) during the immobilization of PEI and T_{48} on a bare silicon oxynitride surface. (C) Layer thickness of A_{48} or T_{48} as a function of the respective mass loading during the entire process of each adsorption from panels A and B. (D) Layer RI of A_{48} or T_{48} as a function of the respective mass loading during the whole process of each adsorption from panels A and B.

charged polycation), providing a surface with positive charges. Then, the negatively charged ssDNA (A_{48} or T_{48}) was adsorbed electrostatically onto the cationic immobilized surface (Scheme 1). The electrostatic attachment of polyanionic PEI on silicon oxynitride surface and subsequent polycationic DNA immobilization was monitored in a real-time fashion by DPI (Scheme 1).

Figure 1A,B displays the time-dependent evaluation of thickness, mass, and RI for the entire ssDNA immobilization process. Derived from Figure 1A,B, moreover, the changes in layer thickness or RI are also plotted as a function of the mass loading of A_{48} or T_{48} (see Figure 1C,D) in order to clearly quantify the extent of ssDNA layer changes. As can be seen from Figure 1A,B, upon addition of PEI, the initial adsorption rate was very fast, during which a sharp increase in thickness and mass loading was accompanied by a rapid decrease in RI, strongly indicating the binding of PEI to the unmodified silicon oxynitride surface. During an incubation period of 5 min, the mass, thickness, and RI of the PEI layer increased at a fast rate to a stable value, suggesting further adsorption of PEI due to the structural and orientational rearrangements.[54] In addition, all panels of Figure 1 clearly show that after ssDNA (A_{48} or T_{48}) was added to the PEI-adsorbed surface, ssDNA started to be adsorbed on the surface in a sharply fast fashion with an almost linear increase in thickness and mass loading and decrease in RI, suggesting the tight association of ssDNA with the PEI surface. ssDNA molecules were then slowly adsorbed until surface was almost saturated. After that, a desorption process of ssDNA was observed. This process gave rise to a slow decrease of mass loading and thickness and a slow increase in RI, suggesting that ssDNA underwent structural and orientational rearrangements on PEI immobilized surface.

The three key parameters (RI, thickness, and mass) describing the stable ssDNA−PEI layers are listed in Table 1. As can be noticed in Table 1 and Figure 1, compared with the PEI layer, the ssDNA layers (A_{48} and T_{48}) had lower RI values,

Table 1. Layer Structure for A_{48}/PEI or T_{48}/PEI Layer[a]

layer material	refractive index	thickness (nm)	mass (ng/mm^2)
PEI	1.468 ± 0.012	2.199 ± 0.465	1.645 ± 0.210
PEI + A_{48}	1.442 ± 0.013[b]	3.985 ± 0.759[b]	2.398 ± 0.257[b]
PEI	1.466 ± 0.015	2.156 ± 0.294	1.599 ± 0.147
PEI + T_{48}	1.462 ± 0.011[b]	3.282 ± 0.598[b]	2.358 ± 0.258[b]

[a]Average ± standard deviation, n = 13. [b]Refractive index, thickness, or mass of the whole A_{48}/PEI or T_{48}/PEI layer.

suggesting that the ssDNA layers were more water-swollen. In addition, the RI of the A_{48}/PEI layer was lower than that of the T_{48}/PEI layer. This might be related to the different interaction of A_{48} or T_{48} with PEI layer. It was previously reported that adenine base possessed larger persistence length and larger hydrophobicity than thymine base,[55,56] and hence A_{48} possibly interacted with PEI layer more weakly than T_{48}, resulting in a looser layer. Caruso and co-workers[57] previously reported that a DNA strand was about 1.9 nm wide. And Hagerman and co-workers[58] pointed out that each base in homoadenine DNA oligonucleotide and homothymine DNA oligonucleotide was approximately 0.32 and 0.52 nm in length, respectively. The lengths of A_{48} and T_{48} were herein calculated to be about 15.36 and 24.96 nm, respectively. Table 1 also clearly shows that after the addition of ssDNA, the thickness of the layer increased by 1.786 nm for A_{48} and by 1.126 nm for T_{48}. The thickness increase values were less than the width value or the length value of A_{48} or T_{48}, suggesting that most A_{48} or T_{48} molecules were likely to lie on the PEI surface in a predominantly "flat-on" conformation and insert themselves partly into the PEI layer. On the other hand, for an A_{48} or a T_{48} molecule, the theoretical saturated surface area per molecule adsorbed on the surface in a "flat-on" conformation was calculated to be about 29.2 and 47.4 nm^2, respectively. The theoretical saturated surface area per molecule for each DNA strand in an "end-on" conformation was approximately equal to 3.6 nm^2 (no matter

dx.doi.org/10.1021/ac2019443 | Anal. Chem. 2012, 84, 924−930

what the sequence or length of DNA).[57] The actual surface area per DNA molecule could be estimated as follows: area per DNA molecule = DNA molecular weight/(DNA mass loading × Avogadro's number). Table 1 lists that the mass loading resolved by DPI was 0.753 ng/mm^2 for A_{48} and 0.759 ng/mm^2 for T_{48}. Given that the molecular weights of A_{48} and T_{48} were 14 972 and 14 539, the actual surface area per molecule for A_{48} and T_{48} was calculated to be about 33 nm^2 and 32 nm^2, respectively. The actual surface area value per molecule for A_{48} was slightly greater than the theoretical saturated area per molecule in a "flat-on" conformation, indicating that A_{48} molecules were very likely to be adsorbed mainly as a flat monolayer on the PEI surface. Moreover, the actual surface area value per molecule for T_{48} was far greater than the theoretical saturated area per molecule in an "end-on" conformation and less than the theoretical saturated area per molecule in a "flat-on" conformation. On the basis of increased values in the layer thickness arising from the addition of T_{48} and the actual surface area value per molecule for T_{48}, we herein suppose that most T_{48} molecules might be inclined to be deposited as a predominantly flat monolayer on the PEI surface.

Coralyne−A_{48} Interaction. Monitoring the binding events between coralyne and A_{48} in a real-time manner allowed kinetic and thermodynamic characterization of the interaction process in detail. Fabrication of the biosensing platform for detection of the interaction of coralyne with A_{48} was displayed in Scheme 1. It can be noticed in Scheme 1 that after A_{48} immobilization, the A_{48}-functionalized anionic surface was challenged with different concentration of coralyne. Coralyne binding to A_{48} was investigated via the aforementioned DPI protocol. The real-time binding data at concentrations of coralyne between 0.5 and 20 μM were collected, and the corresponding real-time mass, thickness, and RI changes are presented in Figure 2. These data clearly show that after the beginning of the addition period, the mass, thickness, and RI begin to rise fast, reach equilibrium, and then return within 300 s almost to the baseline value, indicating the reversibility of the coralyne−A_{48} interaction. From the binding curves of changes in mass, the association (k_a) and dissociation rate (k_d) constants between coralyne and A_{48} were calculated to be 4.95×10^3 $M^{-1}\cdot s^{-1}$ and 0.031 s^{-1}, respectively. Derived from the kinetic constants (k_a and k_d), the association constant (K_A) was 1.6×10^5 M^{-1}, close to the previously reported value of 1.05×10^5 M^{-1}.[46]

Moreover, the increase in layer mass and thickness and the decrease in layer RI can be observed as the concentration of coralyne rises up to 12 μM (Figure 2). Scheme 1 provides a schematic representation of the structural changes of A_{48}/PEI layer arising from the binding of coralyne. It is worth emphasizing that the increase in layer thickness and decrease in layer RI with increasing coralyne concentration are very likely to be mainly due to coralyne inducing the structural change of A_{48} from single-stranded to double-stranded conformation and intercalating into the self-structure, which was in good agreement with those earlier observations that double-stranded DNA formed a thicker but looser layer on top of the polymer layer than single-stranded DNA because of its large size and double-helix rigidity.[39] In addition, at high coralyne concentrations, the binding behavior showed a little difference, especially that the dissociation of coralyne from the A_{48} surface became slower (Figure 2). These differences could be explained either by a more complex binding process or by a rebinding process of coralyne on the surface due to the high surface concentration of binding sites.

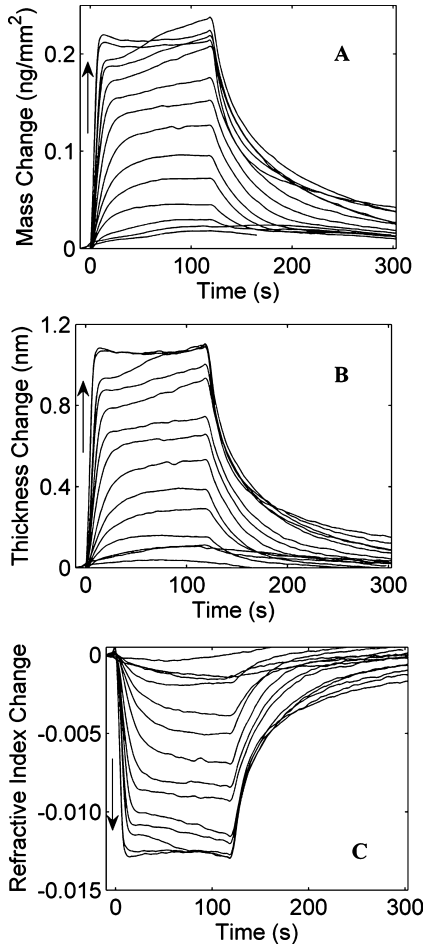

Figure 2. Real-time changes in (A) mass, (B) thickness, and (C) refractive index of the A_{48}/PEI layer as a function of coralyne injections. The arrows show increasing coralyne concentrations: 0.5, 1, 2, 3, 4, 5, 6, 8, 9, 10, 12, 16, and 20 μM.

One significant concern in the direct affinity detection of biomolecular interactions is nonspecific binding to the surface. In this work, as both PEI and A_{48} molecules were attached onto the surface, the nonspecific binding of coralyne to the A_{48}/PEI surface should be evaluated. To effectively discriminate between specific and nonspecific interactions, two control surfaces were fabricated by following a similar protocol to the A_{48}/PEI surface. One was the T_{48}/PEI surface, which was obtained by immobilization of T_{48} on the PEI surface. The other was the PEI surface without immobilization of any ssDNA. Then the two surfaces were interrogated by coralyne at concentrations ranging from 0.5 to 12 μM. A plot of the corresponding changes in mass, thickness, and RI versus coralyne concentration is shown in Figure S4 (Supporting Information). It was found that, upon addition of coralyne, the two control surfaces underwent much smaller changes in mass, thickness, and RI than the A_{48}/PEI surface, and this was particularly clear at higher concentrations of coralyne, indicating the highly specific binding of coralyne, especially at high concentrations, to A_{48}/PEI. Simultaneously, it was clearly observed in Figure S4 (Supporting Information) that the mass, thickness, and RI on the A_{48}/PEI surface at a low coralyne concentration only changed a little, suggesting that the specific recognition of A_{48} by coralyne at low concentrations might be perturbed by PEI.

dx.doi.org/10.1021/ac2019443 | Anal. Chem. 2012, 84, 924−930

Another study confirmed that coralyne intercalated into the self-structure of homoadenine at the level of one coralyne per four adenine bases.[48] In theory, the A_{48} used in the work possessed 12 binding sites for coralyne. The results in Table 1 showed that A_{48} had a mass loading of 0.753 ng/mm^2. Given that A_{48} has a molecular weight of 14 972 and the coralyne molecular weight is 418, the theoretical maximum mass loading of coralyne could be estimated to be approximately 0.25 ng/mm^2. As illustrated in Figure S4A (Supporting Information), the actual mass loading of coralyne was about 0.2 ng/mm^2, which was less than the theoretical maximum mass. The difference in mass loading was most likely related to the fact that A_{48} was immobilized on the silicon oxynitride chip surface through a physically preadsorbed PEI layer. In the physisorbed technique, the PEI layer possibly interfered with the complete binding of coralyne to A_{48}.

Sensitivity and Selectivity of the Coralyne Biosensor. In addition to exploring the interaction between coralyne and A_{48}, we further employed the biosensor for detection of coralyne. The real-time changes in mass, thickness, and RI on the A_{48} surface after addition of coralyne at concentrations ranging from 0.5 to 20 μM are depicted in Figure 2. The corresponding changes in mass, thickness, and RI at 120 s were plotted as a function of the concentration of coralyne (Figure S4, Supporting Information). The results showed that the changes in mass, thickness, and RI were linearly related to the concentration of coralyne ranging from 0.5 to 12 μM. The changes in mass, thickness, and RI could be fitted as $M = 0.019c - 0.017$ (correlation coefficient $r = 0.993$), $T = 0.09c - 0.11$ ($r = 0.993$) and RI $= -0.0016c + 0.0013$ ($r = 0.990$), respectively, where mass M has units of nanograms per square millimeter, coralyne concentration c has units of micromoles per liter (micromolar), and thickness T is given in nanometers. The limits of detection with a signal-to-noise ratio (S/N) of 3 were 0.22 μM for mass calibration, 0.14 μM for thickness calibration, and 0.32 μM for RI calibration, which compared well with values obtained from colorimetric analytical techniques based on gold or silver nanoparticles.[59−61]

In order to assess the specificity of the biosensor for coralyne, we chose three typical intercalators for dsDNA as controls: ethidium bromide (EB), daunomycin (DM), and methylene blue (MB). As shown in Figure S5 (Supporting Information), EB, DM, and MB, caused no noticeable changes in mass, thickness, or RI, demonstrating that the biosensor had a highly selective response to coralyne. The observations simultaneously proved that A_{48} underwent conformational alteration in the presence of coralyne, but no such changes existed in the presence of other intercalators.

CONCLUSION

These investigations gave the first demonstration of application of the DPI technique for probing the interaction of small molecule coralyne with adenine-rich ssDNA in a real-time and label-free manner and for direct, selective, and sensitive detection of coralyne. UV−visible, CD, and DNA melting experiments were performed to demonstrate that 48-mer homoadenine ssDNA oligonucleotide (A_{48}) and 48-mer homothymine ssDNA oligonucleotide (T_{48}) were suitable for the specific recognition element and the control element for coralyne, respectively. These experimental results also confirmed that coralyne could induce the conformational alteration of A_{48} from single-stranded to double-stranded structure and intercalate into the self-structure, but no such conformational change occurred in the presence of T_{48}. The immobilization of ssDNA (A_{48} or T_{48}) on an unmodified silicon oxynitride chip was achieved by a preadsorbed PEI layer. The real-time structural changes in the entire immobilization process could be explained in detail by use of the mass, thickness, and RI data resolved by DPI. The results suggested that most A_{48} or T_{48} molecules were likely to lie on the PEI-adsorbed surface in a predominantly flat monolayer and insert themselves partly into the PEI layer.

Kinetic and thermodynamic parameters characterizing the interaction of coralyne with A_{48} were obtained by monitoring the binding events at different coralyne concentrations. The mass, thickness, and RI changes upon the injection of different concentrations of coralyne allowed qualitative and quantitative analysis of the layer structural changes. The experimental results based on DPI technique indicated that A_{48} likely underwent a conformational change from single-stranded to double-stranded structure in the presence of coralyne. Furthermore, the addition of coralyne at high concentrations gave rise to small structural changes on the two control surfaces (T_{48}/PEI and PEI) but caused noticeable changes on the A_{48}/PEI surface, confirming the specific recognition of A_{48} by coralyne at high concentrations at the solid−liquid interface.

More importantly, three parameters (mass, thickness, and RI) resolved by DPI could be respectively used to establish each calibration equation for the coralyne biosensor. It was found that the biosensor was capable of detecting coralyne over the concentration range from 0.5 to 12 μM with a detection limit of 0.22 μM for mass calibration, 0.14 μM for thickness calibration, and 0.32 μM for RI calibration. The high selectivity of the biosensor to coralyne was confirmed by comparison with three other typical intercalators: ethidium bromide, daunomycin, and methylene blue.

The biosensing strategy we designed in this work offers a new potential avenue for deeply understanding real-time structural aspects of the interactions of target molecules with DNA. This may have important implications for future application of the technique in the discovery of potential therapeutic agents that can selectively target the unique structure of DNA. In addition, it is expected that, combined with SELEX (systematic evolution of ligands by exponential enrichment) technique, the DPI technique may be a valuable tool for allowing rapid generation of new functional DNA molecules (aptamers, DNAzymes, and aptazymes) that exhibit high binding to a variety of target molecules of great interest. By use of these functional DNAs, a spectrum of target molecules such as metal ions, organic molecules, macromolecules, and so on may be detected by the proposed biosensing strategy. Future experiments will be done in our laboratory to validate the proposed biosensing method for detection of various target molecules in real samples.

ASSOCIATED CONTENT

Supporting Information

Additional text describing DPI instrumentation and principle and details of UV−visible and CD experiments; and a figure showing UV−visible absorption spectra of coralyne in the absence and presence of T_{48} or A_{48}; CD spectra of A_{48} or T_{48} with different concentrations of coralyne; CD melting profiles of A_{48} or T_{48} in the presence and absence of coralyne; changes in the mass, thickness, and RI of A_{48}/PEI or T_{48}/PEI or PEI layer upon injection of coralyne at different concentrations; and selectivity of the coralyne biosensor over EB, DM, and MB.

dx.doi.org/10.1021/ac2019443 | Anal. Chem. 2012, 84, 924−930

This material is available free of charge via the Internet at http://pubs.acs.org.

AUTHOR INFORMATION

Corresponding Author

*Telephone: +86 431 85262056. Fax: +86 431 85689278. E-mail: xryang@ciac.jl.cn.

ACKNOWLEDGMENTS

This work was supported by the National Natural Science Foundation of China (21175124, 20890022) and the National Key Basic Research Development Project of China (2010CB933602). We gratefully acknowledge the reviewers for their thorough and thoughtful comments that much improved the manuscript.

REFERENCES

(1) Ahmed, F. E. *Expert Rev. Proteomics* **2008**, *5*, 469−496.
(2) Choi, S.; Goryll, M.; Sin, L. Y. M.; Wong, P. K.; Chae, J. *Microfluid. Nanofluid.* **2011**, *10*, 231−247.
(3) Evans, S. V.; MacKenzie, C. R. *J. Mol. Recognit.* **1999**, *12*, 155−168.
(4) Haseley, S. R. *Anal. Chim. Acta* **2002**, *457*, 39−45.
(5) Cooper, M. A. *Drug Discovery Today* **2006**, *11*, 1061−1067.
(6) Hianik, T.; Wang, J. *Electroanalysis* **2009**, *21*, 1223−1235.
(7) Ince, R.; Narayanaswamy, R. *Anal. Chim. Acta* **2006**, *569*, 1−20.
(8) Neilson, K. A.; Ali, N. A.; Muralidharan, S.; Mirzaei, M.; Mariani, M.; Assadourian, G.; Lee, A.; Van Sluyter, S. C.; Haynes, P. A. *Proteomics* **2011**, *11*, 535−553.
(9) Altschuh, D.; Oncul, S.; Demchenko, A. P. *J. Mol. Recognit.* **2006**, *19*, 459−477.
(10) Zhuang, J.; Cheng, T.; Gao, L. Z.; Luo, Y. T.; Ren, Q.; Lu, D.; Tang, F. Q.; Ren, X. L.; Yang, D. L.; Feng, J.; Zhu, J. D.; Yan, X. Y. *Toxicon* **2010**, *55*, 145−152.
(11) Ju, H. X.; Zhao, H. T. *Front. Biosci.* **2005**, *10*, 37−46.
(12) Li, Z. H.; Hayman, R. B.; Walt, D. R. *J. Am. Chem. Soc.* **2008**, *130*, 12622−12623.
(13) Roth, E. *Pure Appl. Chem.* **1997**, *69*, 1753−1828.
(14) Shi, Y.; Huang, W. T.; Luo, H. Q.; Li, N. B. *Chem. Commun.* **2011**, *47*, 4676−4678.
(15) Cooper, M. A. *Anal. Bioanal. Chem.* **2003**, *377*, 834−842.
(16) Schasfoort, R. B. M.; Tudos, A. J. *Handbook of Surface Plasmon Resonance*; Royal Society of Chemistry: Cambridge, U.K., 2008.
(17) Daniels, J. S.; Pourmand, N. *Electroanalysis* **2007**, *19*, 1239−1257.
(18) Herzog, G.; Arrigan, D. W. M. *Analyst* **2007**, *132*, 615−632.
(19) Vestergaard, M.; Kerman, K.; Tamiya, E. *Sensors* **2007**, *7*, 3442−3458.
(20) Lange, K.; Rapp, B. E.; Rapp, M. *Anal. Bioanal. Chem.* **2008**, *391*, 1509−1519.
(21) Ferreira, G. N. M.; Da-Silva, A. C.; Tome, B. *Trends Biotechnol.* **2009**, *27*, 689−697.
(22) Cross, G. H.; Ren, Y. T.; Freeman, N. J. *J. Appl. Phys.* **1999**, *86*, 6483−6488.
(23) Daghestani, H. N.; Day, B. W. *Sensors* **2010**, *10*, 9630−9646.
(24) Huber, W.; Barner, R.; Fattinger, C.; Hubscher, J.; Koller, H.; Muller, F.; Schlatter, D.; Lukosz, W. *Sens. Actuators, B* **1992**, *6*, 122−126.
(25) Schneider, B. H.; Edwards, J. G.; Hartman, N. F. *Clin. Chem.* **1997**, *43*, 1757−1763.
(26) Freeman, N. In *Proteins at Solid-Liquid Interfaces (Principles and Practice)*; Dejardin, P., Ed.; Springer: New York, 2006.
(27) Karim, K.; Taylor, J. D.; Cullen, D. C.; Swann, M. J.; Freeman, N. J. *Anal. Chem.* **2007**, *79*, 3023−3031.
(28) Swann, M. J.; Freeman, N. J.; Cross, G. H. In *Handbook of Biosensors and Biochips*; Marks, R. S., Lowe, C. R., Cullen, D. C., Weetall, H. H., Karube, I., Eds.; Wiley: New York, 2007.
(29) Swann, M. J.; Peel, L. L.; Carrington, S.; Freeman, N. J. *Anal. Biochem.* **2004**, *329*, 190−198.
(30) Salamon, Z.; Devanathan, S.; Alves, I. D.; Tollin, G. *J. Biol. Chem.* **2005**, *280*, 11175−11184.
(31) Lane, T. J.; Fletcher, W. R.; Gormally, M. V.; Johal, M. S. *Langmuir* **2008**, *24*, 10633−10636.
(32) Khan, T. R.; Grandin, H. M.; Morozov, A. N.; Mashaghi, A.; Textor, M.; Reimhult, E.; Reviakine, I. *Biointerfaces* **2008**, *3*, FA90−FA95.
(33) Mashaghi, A.; Swann, M.; Popplewell, J.; Textor, M.; Reimhult, E. *Anal. Chem.* **2008**, *80*, 3666−3676.
(34) Zhao, X. B.; Pan, F.; Coffey, P.; Lu, H. R. *Langmuir* **2008**, *24*, 13556−13564.
(35) Berney, H.; Oliver, K. *Biosens. Bioelectron.* **2005**, *21*, 618−626.
(36) Lillis, B.; Manning, M.; Berney, H.; Hurley, E.; Mathewson, A.; Sheehan, M. M. *Biosens. Bioelectron.* **2006**, *21*, 1459−1467.
(37) Lee, L.; Johnston, A. P. R.; Caruso, F. *Biomacromolecules* **2008**, *9*, 3070−3078.
(38) Kato, N.; Lee, L.; Chandrawati, R.; Johnston, A, P, R.; Caruso, F. *J. Phys. Chem. C* **2009**, *113*, 21185−21195.
(39) Wang, J.; Xu, X. W.; Zhang, Z. X.; Yang, F.; Yang, X. R. *Anal. Chem.* **2009**, *81*, 4914−4921.
(40) Wang, J.; Coffey, P. D.; Swann, M. J.; Yang, F.; Lu, J. R.; Yang, X. R. *Anal. Chem.* **2010**, *82*, 5455−5462.
(41) Finkel, J. M.; Hill, D. L. *J. Pharm. Sci.* **1978**, *67*, 1331−1332.
(42) Wang, L. K.; Rogers, B. D.; Hecht, S. M. *Chem. Res. Toxicol.* **1996**, *9*, 75−83.
(43) Fox, K. R. *Nucleic Acids Res.* **1992**, *20*, 1235−1242.
(44) Economou, E. P.; Bergen, A. W.; Warren, A. C.; Antonarakis, S. E. *Proc. Natl. Acad. Sci. U.S.A.* **1990**, *87*, 2951−2954.
(45) Joung, I. S.; Cetinkol, O. P.; Hud, N. V.; Thomas, E. *Nucleic Acids Res.* **2009**, *37*, 7715−7727.
(46) Ren, J. S.; Chaires, J. B. *Biochemistry* **1999**, *38*, 16067−16075.
(47) Polak, M.; Hud, N. V. *Nucleic Acids Res.* **2002**, *30*, 983−992.
(48) Persil, O.; Santai, C. T.; Jain, S. S.; Hud, N. V. *J. Am. Chem. Soc.* **2004**, *126*, 8644−8645.
(49) Gibson, D. *Pharmacogenomics J.* **2002**, *2*, 275−276.
(50) Krugh, T. R. *Curr. Opin. Struct. Biol.* **1994**, *4*, 351−364.
(51) Van Amerongen, H.; Van Grondelle, R.; Van der Vliet, P. C. *Biochemistry* **1987**, *26*, 4646−4652.
(52) Johnson, B. B.; Dahl, K. S.; Tinoco, I. Jr.; Ivanov, V. I.; Zhurkin, V. B. *Biochemistry* **1981**, *20*, 73−78.
(53) Shovsky, A.; Bijelic, G.; Varga, I.; Makuška, R. A.; Claesson, P. M. *Langmuir* **2011**, *27*, 1044−1050.
(54) Zhao, X. B.; Zhang, Z. Q.; Pan, F.; Ma, Y. H.; Armes, M. P.; Lewis, A. L.; Lu, J. R. *Langmuir* **2005**, *21*, 9597−9603.
(55) Mills, J. B.; Vacano, E.; Hagerman, P. J. *J. Mol. Biol.* **1999**, *285*, 245−257.
(56) Akca, S.; Foroughi, A.; Frochtzwajg, D.; Postma, H. W. C. *PloS One* **2011**, *6*, No. e18442.
(57) Johnston, A. P. R; Read, E. S.; Caruso, F. *Nano Lett.* **2005**, *5*, 953−956.
(58) Mills, J. B.; Vacano, E.; Hagerman, P. J. *J. Mol. Biol.* **1999**, *285*, 245−257.
(59) Xu, X. W.; Wang, J.; Yang, F.; Jiao, K.; Yang, X. R. *Small* **2009**, *5*, 2669−2672.
(60) Lv, Z. Z.; Wei, H.; Li, B. L.; Wang, E. K. *Analyst* **2009**, *134*, 1647−1651.
(61) Song, G. T.; Chen, C.; Qu, X. G.; Miyoshi, D.; Ren, J. S.; Sugimoto, N. *Adv. Mater.* **2008**, *20*, 706−710.